

# Computerized Planning of Cryosurgery: From Model Reconstruction to Cryoprobe Placement Strategies

Yoed Rabin\*

Department of Mechanical Engineering, Carnegie Mellon University,  
5000 Forbes Avenue, Pittsburgh, PA 15213

## ABSTRACT

As a part of an ongoing program to develop computerized tools for surgery, the current study focuses on the design of optimal cryoprobe layouts for prostate cryosurgery. Once a decision to treat the prostate with cryosurgery has been made, its application can be presented as a four-stage process: (i) 3D reconstruction of the target region; (ii) evaluation of the optimum number of cryoprobes and their layout; (iii) insertion of cryoprobes according to that plan; and, (iv) orchestrating cryoprobe operation to achieve the optimum match between the target region and the forming frozen region. Cryosurgical success equals the sum of the successes of each of the above stages. To date, this four-stage process is performed manually, relying upon the cryosurgeon's experience and "rules of thumb". This manuscript reviews recent efforts to develop the necessary building blocks for an integrated computerized surgical tool for prostate cryosurgery, which includes methods for prostate model reconstruction, schemes for bioheat transfer simulation, and optimization techniques for cryoprobe placement; experimental verification of these building blocks are also presented. The emphasis in this line of development is on performing a full-scale planning in less than one minute, while the patient is on the operation table. It can be concluded from the current manuscript that the above goals are achievable. The current manuscript concludes with a review of current challenges in the development of related computerized means.

**Keywords:** Cryosurgery, Computerized Planning, Prostate, Bioheat Simulations, Optimization, Model Reconstruction

## 1. INTRODUCTION

Cryosurgery is the destruction of undesired biological tissues by freezing. While tissue injury at low temperatures is known since the dawn of history, the application of refrigeration systems to focused tissue destruction was introduced only at the late 19<sup>th</sup> century, with the introduction of liquefied air [27]. Cryosurgery began to develop as an invasive surgical technique in 1961, when Cooper and Lee invented the modern liquid-nitrogen-based cryoprobe [4], where nitrogen boiling is essentially the driving mechanism of cooling. A popular cooling alternative to nitrogen boiling is the cooling effect associate with the sudden expansion of a compressed gas, also known as the Joule-Thomson effect [16]. While the Joule-Thomson effect is known since the middle of the 19<sup>th</sup> century, it was less popular as a cooling mechanism in earlier cryodevice developments, due to its inferior cooling power and due to potential complications associated with the highly compressed gasses in an invasive surgical tool (this pressure is measured in thousands of psi).

As a minimally-invasive procedure, cryosurgery was first introduced in the early 1980s for the treatment of the prostate cancer. However, it was not until the early 1990s that technological developments allowed for the procedure to pass from the experimental stage to the stage of routine clinical practice [9]. With continuous efforts to decrease the cryoprobe size, while compromising on an increased number of cryoprobes, the Joule-Thomson-based cryoprobes became more popular than boiling-effect-based cryoprobes in recent years. The best cooling mechanism for cryosurgery remains open for debate, as the technology of cryosurgery continues to develop, where related discussions are beyond the scope of the current manuscript.

Today, minimally-invasive prostate cryosurgery is performed with the application of multiple cryoprobes, in the shape of long hypodermic needles, strategically located in the region to be destroyed [6]. Currently, cryoprobe localization is an art held by the cryosurgeon, based on the surgeon's own experience and accepted practices. Once localized, cryoprobes are operated in a trial-and-error fashion, until the entire target volume is believed to be frozen. The cryosurgeon monitors the procedure by means of medical imaging—such as ultrasound or MRI [9,10,21,22]—and adjusts the cooling power of

---

\* Email: [rabin@cmu.edu](mailto:rabin@cmu.edu); Phone/Fax: (412) 268 2204; <http://www.me.cmu.edu/BTTL.htm>

the individual cryoprobes accordingly to best match the area to be treated with the developing frozen region.

Prostate cryosurgery often involves two freezing/thawing cycles, where the cryoprobes are retracted between cycles—also known as the “pullback procedure.” The pullback procedure is aimed at improving the match between the area to be treated and the shape of the developing frozen region. The pullback procedure should be distinguished from multiple freezing/thawing cycles without cryoprobe relocation (which was more popular at earlier phases of cryosurgery development) in order to increase the likelihood of tissue destruction at the expense of an elongated operation time. Suboptimal cryoprobe placement may lead to portions of the target region being insufficiently cryotreated, cryoinjury to the healthy surrounding tissues, and elongated surgical operation, all of which affect the quality and the cost of the medical treatment. Computerized planning tools can help alleviate these difficulties by identifying an optimal cryoprobe layout and by providing close to real-time prediction of the resulting thermal field, with the match between the target region and the frozen region being one measure of the quality of planning. It is the development of computer-assisted planning to identify the optimal cryoprobe layout which is the core of our ongoing research program.

A limited number of studies have addressed the need to develop computerized means to improve cryosurgical planning [1,2,7]. While these studies proposed various planning techniques, they were all associated with a high computational cost, thus preventing their practical application. Alternative methods for computerized planning of cryosurgery have been developed by our research team, with the so-called “force-field analogy” being the most robust, but also the most computationally expensive of those developments [8,15]. More recently, the so-called “bubble-packing” method has been developed, with the objective of identifying the best initial condition for the force-field analogy method [23]. The high quality of the cryoprobe layout at the end of the bubble-packing phase of planning, together with its relatively low computational cost, have made the need for a second-phase of planning (i.e., the force-field analogy) debatable in some cases [24].

This manuscript reviews recent efforts to develop the necessary building blocks for an integrated computerized surgical tool for prostate cryosurgery, which includes a technique for geometric modeling of the target region based on ultrasound imaging, a numerical technique for cryosurgery simulations, cryoprobe layout planning algorithms (the so-called force-field analogy and the bubble-packing method), and experimental verification of developed computerized means. The current manuscript concludes with a review of current challenges in the development of related computerized means.

## 2. GEOMETRIC MODELING

One of the key difficulties in developing real-time planning tools for cryosurgery is the reconstruction of a target region model. Cryosurgery is typically performed under the guidance of a single trans-rectal ultrasound transducer (TRUST), which is the only imaging technique currently approved by health insurance companies in the USA for the treatment of the prostate cryosurgery. With the application of a registration mechanism—for the rotational and translational movement of the transducer—the ultrasound imaging technique can be adequately used for preplanning. Since no compatible model reconstruction technique is currently available, a data bank of five prostate was established in the course of this project, based on preclinical ultrasound scanning.

The method of model reconstruction is discussed in detail elsewhere [24,28], and is presented below in brief only, for the completeness of presentation. Each preclinical data set (e.g., a prostate and its surrounding organs) included a gray-scale array of pixels having an average size of 813 (longitudinal)×413×336. The 3D shape of a prostate is reconstructed based on manual segmentation of ultrasound images. The user selects a series of good quality ultrasound images of a transverse cross section, from the apex to the base of the prostate, as illustrated in Fig. 1(a). On each cross section, the user identifies the contour of the prostate as a sequence of points, having a denser distribution for a high-curvature part of the contour. Next, the points are connected to form a polyline, which is then approximated as a piecewise cubic Bezier curve. In order to form a smooth contour, two adjacent curves are forced to share the same end point. Furthermore, two additional control points are added so that the slopes of the two adjacent curves become continuous. This procedure is repeated for all the selected cross sections, resulting in a series of transverse contours, as illustrated in Fig. 1(b).

Once a series of transverse contours is generated, a series of longitudinal cross sections is defined, intersecting perpendicularly with all the transverse contours. Points from all the intersected transverse contours are connected along each longitudinal cross section—to form a series of longitudinal polylines running from the apex to the base of the

prostate. In a similar manner to the process of generating of the transverse contours, each longitudinal polyline is approximated as a piecewise cubic Bezier curve, and continuity of position and slope is forced at the end of each curve to ensure the smoothness of the contour. Finally, the surface of the prostate is presented with a polygonal mesh based on bi-cubic Bezier surface interpolation, as illustrated in Fig. 1(c).

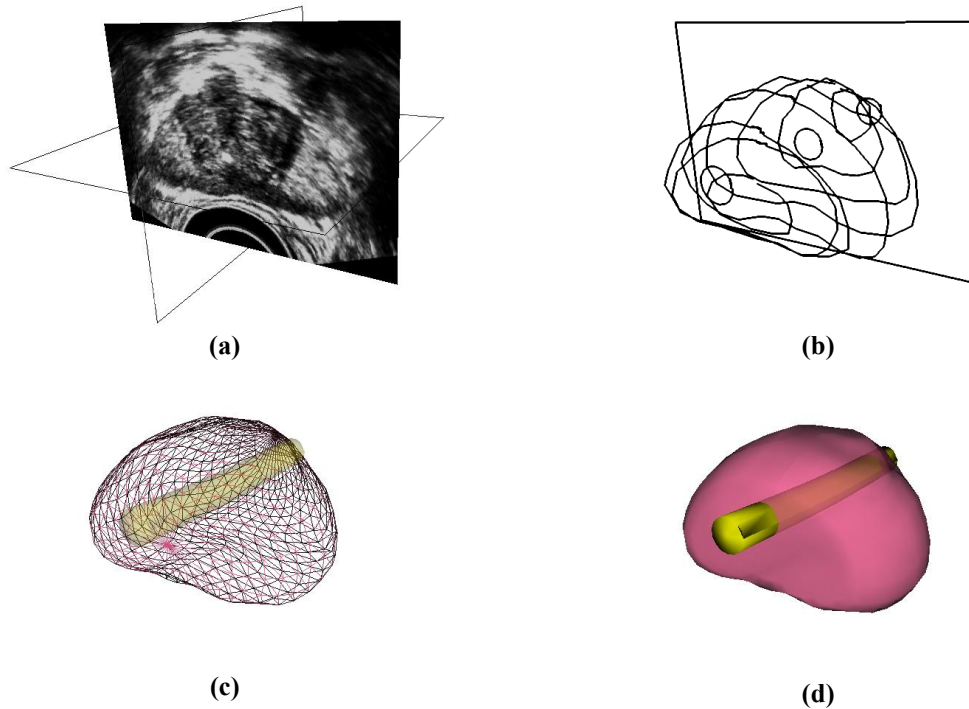


**Figure 1:** Reconstruction of the prostate model from ultrasound images: (a) selection of good quality ultrasound cross sections; (b) generation of the prostate contour on each cross section, including illustration of the urethral warmer; (c) generation of polygonal mesh based on cubic Bezier surface interpolation; and, (d) surface rendering of the prostate [24] (movies on the process are displayed in [28]).

Consistent with current prostate-cryosurgery practice, a urethral warmer is assumed in the prostate, although not originally present in the ultrasound image data. This warmer, embedded in a catheter, is ordinarily inserted into the urethra to keep its temperature above freezing, and thereby to reduce post-cryosurgery complications [11]. In the current study, the geometry of the urethral warmer is modeled as a 6 mm-diameter tube, having the same centerline as the urethra, as identified from ultrasound images. The shape of the urethral warmer is modeled by connecting 6 mm-diameter circles from each image, in a similar manner to the outer prostate surface reconstruction.

### 3. CRYOSURGERY SIMULATION

A key element in cryosurgery planning is the ability to predict (i.e., simulate) the resulting temperature field for a given geometrical model (i.e., the prostate) and for a specific cryoprobe layout. Review of the simulation technique for a given cryoprobe layout is given below, whereas techniques for how to improve the cryoprobe layout are discussed in next section of this manuscript. In general, there are numerous simulation techniques for heat transfer involving phase change, as is the case with cryosurgery, ranging from tailor-made techniques to meet particular benchmarks [13] to commercial codes (e.g. ANSYS, Inc., and SIMULIA, Inc.), which are robust and versatile. Despite many advantages of commercial codes, their major drawback is their long runtime, which is typically the trade-off for robustness.

For the purpose of the current project, a finite-difference numerical technique has been developed, with the goal of simulation runtime under one minute [18]. The numerical scheme solves the classical bioheat transfer problem in the tissue:

$$C \frac{\partial T}{\partial t} = \nabla \cdot (k \nabla T) + w_b C_b (T_b - T) + q_{met} \quad (1)$$

where  $C$  is the volumetric specific heat of the tissue,  $T$  is the temperature,  $t$  is the time,  $k$  is the thermal conductivity of the tissue,  $w_b$  is the blood perfusion volumetric flow rate per unit volume of tissue,  $C_b$  is the volumetric specific heat of the blood,  $T_b$  is the blood temperature entering the thermally treated area, and  $q_{met}$  is the metabolic heat generation.

Numerous scientific reports have been published studying the mathematical consistency and validity of the above classic equation, while exploring various alternatives [3,5]. It is assumed in the current study that a more advanced model of bioheat transfer will not warrant higher accuracy in the cryosurgery simulation, it will involve greater mathematical complications, and is deemed unnecessary in the current study. Note that metabolic heat generation is typically negligible compared to the heating effect of blood perfusion, and is therefore neglected in this study [19]. Table 1 lists typical values of the thermophysical properties used in the course of developing the planning tools. For this numerical scheme, it is assumed that the specific heat is an effective property within the phase transition temperature range of  $-22^\circ\text{C}$  to  $0^\circ\text{C}$  (the tissue is first order approximated as an NaCl solution), where a detailed discussion about the application of the effective specific heat to phase-change problems is given by Rabin and Korin [11].

**Table 1:** Representative thermophysical properties of biological tissues used in the current study [15].

Thermophysical Property	Value	
Thermal conductivity, $k$ , W/m-K	0.5	$273\text{K} < T$
	$15.98 - 0.0567 \times T$	$251\text{K} < T < 273\text{K}$
	$1005 \times T^{-1.15}$	$T < 251\text{K}$
Volumetric specific heat, $C$ , MJ/m <sup>3</sup> -K	3.6	$273\text{K} < T$
	$880 - 3.21 \times T$	$265\text{K} < T < 273\text{K}$
	$2.017 \times T - 505.3$	$251\text{K} < T < 265\text{K}$
	$0.00415 \times T$	$T < 251\text{K}$
Blood perfusion, $w_b C_b$ , kW/m <sup>3</sup> -K	40	

Equation (1) can be rewritten in a finite-difference form [18]:

$$T_{i,j,k}^{p+1} = \frac{\Delta t}{\Delta V_{i,j,k} [C_{i,j,k} + (w_b C_b)_{i,j,k} \Delta t]} \sum_{l,m,n} \frac{T_{l,m,n}^p - T_{i,j,k}^p}{R_{l,m,n-i,j,k}} + \frac{\Delta t [(w_b C_b)_{i,j,k} T_b + (q_{met})_{i,j,k}] + C_{i,j,k} T_{i,j,k}^p}{C_{i,j,k} + (w_b C_b)_{i,j,k} \Delta t} \quad (2)$$

where  $i,j,k$  and  $l,m,n$  are space indexes,  $p$  is a time index,  $\Delta V$  is an element volume associated with a grid point,  $\Delta t$  is a time interval, and  $R$  is the thermal resistance to heat transfer by conduction between node  $i,j,k$  and its neighbor  $l,m,n$ . Equation (2) is rather general, and its formulation is independent of the coordinate system.

The numerical scheme presented in Eq. (2) is conditionally stable, which is its most significant disadvantage. Hence, the application of this numerical scheme calls for careful discretization in space and time, to ensure its most efficient use as discussed by Rossi et al. [18]. For the efficient application of this numerical method, a scheme based on variable grid spaces and variable time intervals has been developed [18]. Analysis of that numerical technique in 1D suggested that 1 mm intervals can be considered adequate for the fine grid around the cryoprobes, when only two grid levels are applied. Analysis in 2D suggested that a ratio of 1:3 between the fine grid and the coarse grid can be considered adequate. Analysis in 3D suggested that a simulated domain containing the prostate model can be considered infinite in the thermal sense when its cross-sectional area is 3.5 times larger than the largest prostate cross-sectional area (perpendicular to the direction of insertion of cryoprobes), and when its length is 1.5 times longer than the prostate.

Analyses in 2D and 3D showed that increased grid size causes the freezing front to lag correspondingly. Nevertheless, it was demonstrated that the best cryoprobe layout is independent of that time lag, which confirms that the numerical scheme is suitable for the optimization techniques reviewed in the next section of this manuscript. Heat transfer simulation in 3D, using grid ratios of 1:2 and 1:3 showed decreased runtime by a factor of 24 and 40, respectively, bringing the simulation runtime to a desired range of 1 to 2 min. This typical runtime in 3D enabled the progression of the project to the development of planning algorithms.

## 4. CRYOPROBE LAYOUT PLANNING

The objective of the planning tool is to determine the best locations to insert the cryoprobes based on bioheat transfer simulations. Two algorithms have been developed to achieve this task termed “force-field analogy” [8] and “bubble packing” [23]. While the bubble-packing method has been developed as a technique to find an initial condition for the robust force-field analogy method [23], the bubble-packing method was later found efficient enough as a planning scheme when executed alone. The principles of each of these planning methods are overviewed below. It is noted that the presented planning schemes are general and suitable for application with any cryosurgery hardware.

### 4.1 Force-Field Analogy

The force-field analogy procedure employs a novel iterative optimization technique [8]. Each iteration starts with a single transient bioheat transfer simulation of the cryoprobe, based on a proposed cryoprobe layout. At the end of the simulation, regions of tissue that would have undesired temperatures apply “forces” to the cryoprobes, directly moving them to better locations, and a new cryoprobe layout is prepared for the consecutive iteration. The process of simulations and cryoprobe relocation continues until no improvement can be made in the cryoprobe layout. This method is more efficient than traditional numerical optimization techniques since, in principle, all the cryoprobe can be relocated between every two consecutive heat transfer simulations, resulting in a dramatic decrease in the number of bioheat transfer simulations. Figure 2 is presented for illustration purposes, where the circular 2D target region is simulative of the prostate cross section.

Consistent with current practice, the objective of planning is to best match an isothermal for planning with the shape of the target region. For illustration purposes, the  $-22^{\circ}\text{C}$  isotherm is selected, splitting the temperature range between the onset of freezing and the so-called lethal temperature. At the end of each simulation, defects in the temperature field are identified, where a defect is defined as either internal area to the target region above the planning isotherm, or external to the target region below the same isotherm. The temperature regions at the end of the first simulation are illustrated in Fig. 2(a) and the defect regions are displayed red in Fig. 2(b).

At the end of the simulation, forces proportional to the size of defect are computed:

$$\bar{F}_{nT} = \sum_m \frac{C_1}{|\bar{r}_{mn}|^2} w_m A_m \Delta T_m \bar{u}_{mn} \quad (3)$$

where  $C_1$  is a constant,  $r_{mn}$  is the distance between a cryoprobe and the center of mass of the defect,  $w_m$  is a weight function (a value of +1 for an external defect representing repulsion and a value of -1 for an internal defect representing attraction),  $A_m$  is the size of the defect,  $\Delta T_m$  is the temperature difference between the defect and the planning isotherm, and  $u_{mn}$  is a unit vector pointing from the cryoprobe to the center of mass of the defect. These forces are illustrated as vectors in Fig. 2(a). Next, cryoprobes are relocated in the direction of forces, to a distance proportional to the force magnitude. In order to prevent cryoprobe congestion due to geometrical consideration, similar repulsion forces between cryoprobes are also calculated. While the force-to-defect value calculated by Eq. (3) is inversely proportional to the distance squared, the repulsion forces between cryoprobes are inversely proportional to the distance cube, which makes repulsion forces between cryoprobes effective only in short distances.

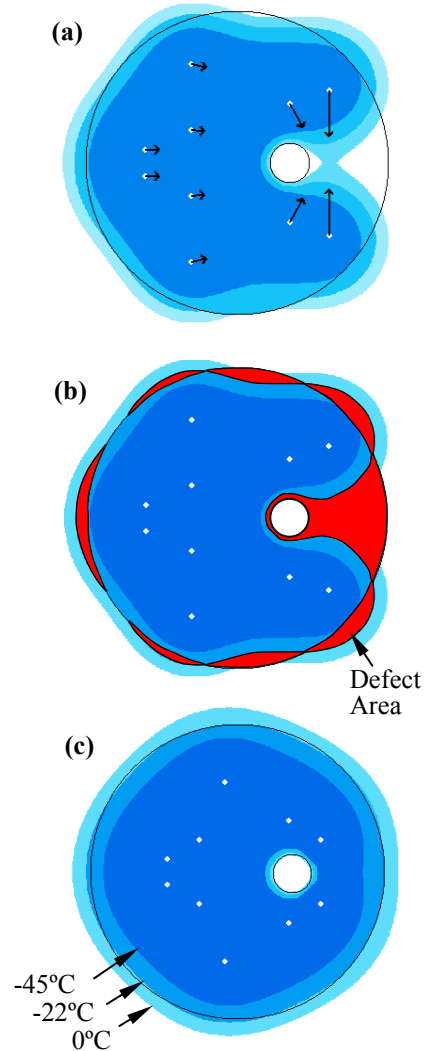


**Figure 2:** Planning starting from a random initial configuration in a 2D-circular target region. Cryoprobes are represented as white circles. (a) The temperature regions and forces on cryoprobes at the end of the first simulation. (b) Defects (red areas) at the end of the first simulation. (c) The temperature regions at the end of the final simulation for the optimal configuration [8].

The process of bioheat simulations and cryoprobes relocation continues as necessary, until the overall defect value in the system reaches minimum, as displayed in Fig. 2(c). There is no limit to the number of cryoprobes which can be relocated after one bioheat simulation, which is the major advantage of the force-field analogy method over an ordinary gradient-decent method. In a gradient-decent method only one cryoprobe can be moved at a time, a decision which requires three bioheat simulations in a 3D case. Taking into account up to 14 cryoprobes in a typical prostate cryosurgery, an ordinary gradient-decent method is impractical, even if each simulation takes only one minute (see Section 3, above). Results of force-field planning in 2D and 3D are presented in [8,15,23].

#### 4.2 Bubble-Packing Method

While the force-field analogy method has been shown robust with an outcome insensitive to the initial condition, the number of iterations required to find a global minimum on the defect is dependent on the initial condition. In order to accelerate computer planning, the bubble-packing method has been developed, with the goal of generating a uniform initial distribution of cryoprobes. Unlike the force-field analogy, the bubble-packing method does not incorporate bioheat transfer simulations.

Bubble packing is a physically based approach that efficiently finds the even distribution of an arbitrary number of points inside a given geometric domain. The method first generates spherical elements—bubbles—inside that domain. Next, van der Waals-like forces are assumed to drive bubbles, until a minimum energy configuration of bubbles is reached. In broad terms, the van der Waals model represents proximity-based forces between every two elements in the domain. An attraction force is applied when the two elements are too distant from one another, while a repulsion force is applied when they are too close. Only one distance exists where these forces equilibrate. Once bubbles are seeded (or, mathematically defined in the domain), their forced motion is simulated until all inter-bubble forces equilibrate. In the current study, the van der Waals-like forces are defined as:

$$f(l) = \begin{cases} \alpha l^3 + \beta l^2 + \gamma l + \varepsilon & 0 \leq l \leq 1.5l_0 \\ 0 & 1.5l_0 < l \end{cases} \quad (4)$$

subject to the boundary conditions of:

$$f(l_0) = f(1.5l_0) = 0, \quad f'(0) = 0, \quad f'(l_0) = -\kappa_0 \quad (5)$$

where  $l$  is the distance between the two bubbles,  $l_0$  is the distance of force equilibrium between two isolated bubbles,  $\kappa_0$  is the approximated linear spring constant at a distance  $l_0$ ;  $\alpha$ ,  $\beta$ ,  $\gamma$ , and  $\varepsilon$  are force constants.

The motion of bubbles towards equilibrium is simulated as a force-relaxation process:

$$m_i \frac{d^2 x_i(t)}{dt^2} + c_i \frac{dx_i(t)}{dt} = f_i(t) \quad (6)$$

where  $x_i$  is the location of the  $i^{\text{th}}$  bubble, while  $m_i$  and  $c_i$  denote the virtual mass and damping coefficient of the  $i^{\text{th}}$  bubble, respectively;  $m_i$  and  $c_i$  are assumed from computational convergence consideration, but their actual values have no physical meaning in the context of cryosurgery. Note that  $f_i(t)$  is the sum of all inter-bubble forces working on the  $i^{\text{th}}$  bubble. Equation (6) is numerically integrated using a fourth-order Runge-Kutta method. Finally, the volume of the bubbles is adjusted to both minimize the gap between bubbles and prevent bubble overlapping when force relaxation progresses with the change in bubble size.

Insight on the application of bubble packing to cryosurgery planning are presented in [19,23-26]. See also movies at [30].

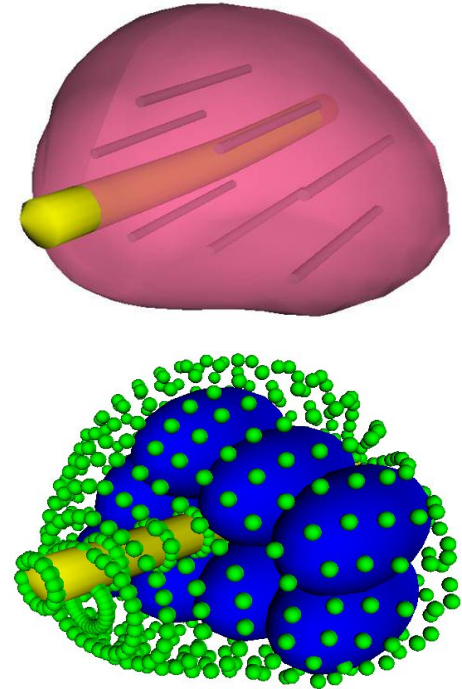


**Figure 3:** Illustration of boundary representation for bubble packing: the contour of the reconstructed prostate model (top) is replaced with boundary bubbles (small bubbles—bottom), and cryoprobe representing bubbles (large bubbles) are packed in the domain; the size of the infinitesimal boundary bubbles is enlarged for illustration purposes. The active surfaces of cryoprobes are also illustrated (top), based on the bubble packing results [25].

## 5. EXPERIMENTAL VERIFICATION

Two objectives have been set for the experimental work in this ongoing research: (i) to verify that the proposed numerical scheme (Section 3, above) can reliably capture the temperature field in the frozen region [17], and (ii) to verify the ability to automatically selected an adequate cryoprobe layout for cryosurgery using computerized means (Section 4, above) [19]. While the computerized planning means are essentially 3D in nature, experimental verification is focused on 2D for practical reasons with the overriding goal of increasing certainty in comparison between experimental data and simulation results.

### 5.1 Experimental Setup

A detailed description of the experimental system is discussed in [17], and is presented here in brief only, for the completeness of presentation. The experimental setup is designed for 2D cryosurgery simulations on a gelatin solution as a phantom material, where the 2D setup is representative of a prostate cross-section (Fig. 4, top image). The thermophysical properties of pure water are close to those of soft tissues, and the gelatin is added to prevent convective heat transfer in the domain. In order to accentuate the contrast between the frozen and unfrozen regions in the gelatin, blue food dye was added at a concentration of about 0.4 ml/liter.

A proprietary cryodevice was used in the current study, which is a modification of an earlier liquid-nitrogen-based device [12]. The new cryoprobes are similar to the original cryoprobes invented by Cooper and Lee [4], with the exception of an off-center internal tube, and an embedded T-type thermocouple in the outer wall. The tubes are made of copper, the external diameter of the inner and outer tubes are 1.6 mm and 3.2 mm, respectively, and a wall thicknesses are 0.4 mm. Up to six cryoprobes were connected to the liquid nitrogen supply system. Experiments were conducted subject to a relatively low-pressure liquid-nitrogen supply of less than 20 psi. Simultaneous operation of six cryoprobes under this pressure led to a cooling rate of about  $33^{\circ}\text{C}/\text{min}$  in the first three minutes of operation, and a minimum operation temperature of about  $-110^{\circ}\text{C}$ . Increasing the pressure would dramatically increase the cooling rate, while decreasing the minimum temperature towards the liquid nitrogen boiling temperature of  $-196^{\circ}\text{C}$  [12]. However, such an increase in pressure would result in a significant decrease in the thermal efficiency of the system [12].

Urethral warming was simulated with a cryoheater [14,15], which is a self-controlled electric heater, embedded either in a hypodermic needle or in a catheter. Embedded in a catheter, the cryoheater is an alternative to the common urethral warmer, made of a double-pipe water heat exchanger (shown in Fig. 4). The cryoheater in that study was placed inside a 7 mm OD thin-wall brass tube, and a T-type thermocouple was embedded in the wall of

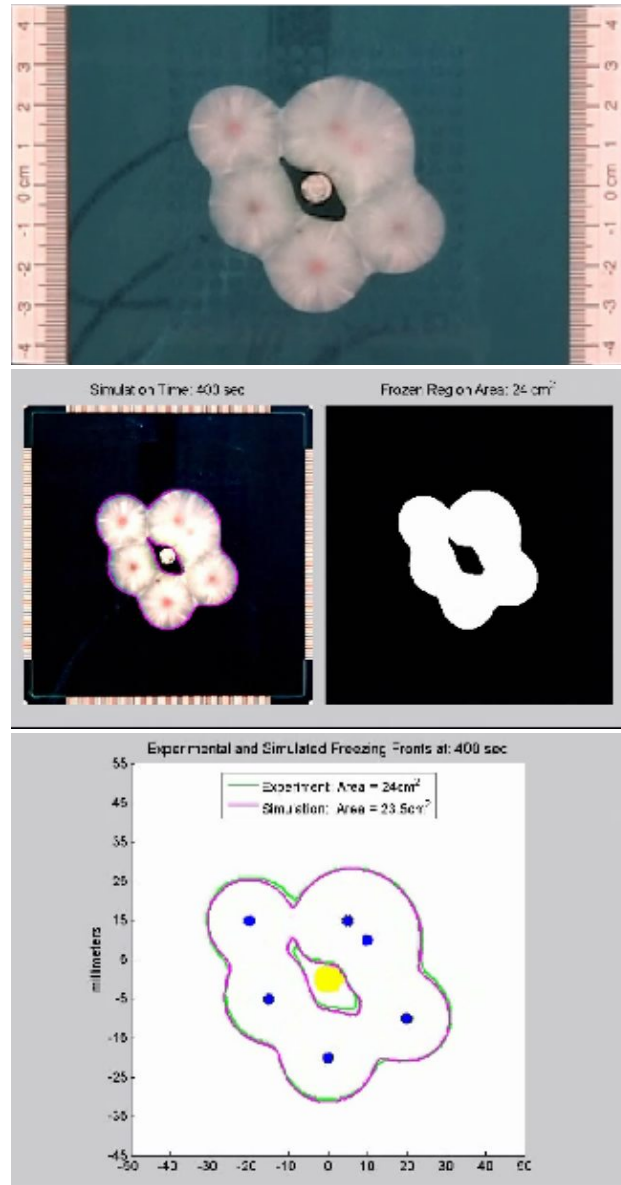


**Figure 4:** Comparison of experimental data with simulation results: (top) an image of the 2D frozen region, generated by 6 cryoprobes around a cryoheater; (middle-right) segmented frozen region; (middle-left) the contour of the segmented frozen region—pink—superimposed on an enhanced image of the frozen region; (bottom) comparison of simulated results with reconstructed freezing front contour. Images are presented after 400 seconds from the beginning of freezing, long before the freezing process reaches steady state.

the cryoheater, for thermal control purposes. A cryogenic controller and a power supply in one unit were used to maintain the temperature of the urethral warmer constant throughout the experiment (Cryocon, Model 32).

Experiments were conducted in a Plexiglas container, having a gelatin chamber of 25 mm × 200 mm × 200 mm. A grid of 15 × 15 holes with 5 mm intervals was drilled in one side of the container to accommodate the cryoprobes (3.2 mm in diameter). A 7 mm in diameter hole was drilled at the center of the grid to accommodate the cryoheater. Temperature data from the cryoprobes and the cryoheater was collected through a USB data acquisition system (Omega, OMB-DAQ-56) and computer-recorded. Experiments were also video-recorded (Canon ZR300 Mini DV camcorder); the camcorder was placed on a special stage, approximately 0.7 m from the container.

## 5.2 Experimental Results for Freezing Front Location

Analysis of experimental results focused on two key measurements: comparison of measured and simulated temperatures at strategically located points, and comparison of freezing front location between experiments and simulations. For this purpose, a special algorithm was developed to extract the freezing front location from video recording of the freezing process. Here, the video recording was processed by extracting one image (a snapshot) per second (Fig. 4, top). The contrast of the image was enhanced with Adobe Photoshop 7.0 (Fig. 4, middle-left), and the image was then converted from a true color RGB image to an 8 bit grayscale image. The contrast was further enhanced using the Matlab filter “unsharp.” Due to the high contrast level achieved, a relatively simple region-growing segmentation technique was then applied, starting at seed points located at the centers of the cryoprobes. Neighboring pixels were evaluated based on intensity level and proximity to previously added pixels. Upon completion of the region-growing algorithm, a dilation transformation was performed to enlarge the segmented image and to fill in small holes and gaps (Fig. 4, middle-right). Finally, segmentation and simulation results for the freezing front location were compared (Fig. 4, bottom). Movies of the process for eight typical cases are posted on the web [29].

A total of 24 experiments are reported in [17], and in eight representative cryoprobe layouts, where three experiments were repeated on each layout. Results indicate defect areas of less than 5%, with an average value of 2.9%, between experimental data and simulation results. Results further indicate an average uncertainty of 0.4 mm in freezing front location.

Uncertainty of not less than 1 mm in identifying the prostate contour is probably a lower boundary, when using a single rectal ultrasound transducer during prostate cryosurgery. In fact, due to the typical quality of ultrasound imaging, some surface areas of the organ are interpolated based on imaging data, rather than directly extracted from imaging. Given the quality of agreement between experimental data and numerical simulations presented in the current study, the typical quality of organ reconstruction for cryosurgery applications, and the fact that the defect area concept is the key for computerized planning in parallel studies, it is concluded that the numerical technique presented in Section 3 of the current manuscript is adequate for the purpose of computerized planning of prostate cryosurgery, using the prototype algorithms presented in Section 4 of the current manuscript.

## 5.3 Experimental Results for Optimum Cryoprobe Layout

Due to the high quality of bubble-packing planning, and the marginal improvement of the force-field analogy planning over bubble packing, experimental verification of computerized planning was focused on bubble packing alone [19]. In order to increase the quality of bubble-packing planning, three modifications have been made to the original scheme: attractive forces were eliminated, the overlap ratio between bubbles was increased, and the radius of boundary bubbles was increased from an infinitesimal value to 4 mm. These modifications are related to the parameters most affecting the quality of planning; however, the scheme can further be optimized for increased quality.

Bubble-packing planning was compared with experimental results from six different experimental layouts, at three points in time for each experiment, yielding a total of 18 cases. For each case, the target region for planning was defined as the reconstructed shape of the frozen region, taken from video recording of the experiment, using a reconstruction methodology published recently. Using the defect region concept, bioheat transfer simulations were used to evaluate the quality of the cryoprobe layout suggested by bubble packing, in comparison with the experimentally applied cryoprobe layout. Results indicate defect areas of less than 8% and an average value of 6.1%. This defect corresponds to an average mismatch of 0.8 mm between the freezing front and the contour of the target region, where the freezing front is the control variable used by clinicians for imaging-guided cryosurgery. For ultrasound imaging, where an uncertainty value

of 1 mm is commonly accepted as a reasonable value for identification of the freezing front or a contour of an organ, prediction of the freezing front within a certainty of 0.8 mm is deemed adequate. Based on experimental results on gelatin, it is concluded that bubble-packing planning is an efficient means to identify an optimal cryoprobe layout.

Results of this study support the previously made observation that—in contrast to a common argument made by cryodevice manufacturers—the quality of planning is not affected significantly by the number of cryoprobes beyond some threshold number. The overall freezing time however, is affected by the number of cryoprobes. When evaluating these observations, the additional trauma resulting from the increased number of cryoprobes must be taken into consideration, an effect which was not studied here.

## 6. CURRENT CHALLENGES

Dramatic developments in imaging, instrumentation, and computational techniques in recent years have opened new horizons for the application of multi-probe and minimally invasive cryosurgery. Commercial cryoprobes are now available that are as narrow as 1 mm in diameter, and in a wide range of active lengths. These small diameters, and the variability in active length, can potentially improve the surgeon's control over the minimally invasive procedure. In prostate cryosurgery for example, up to 14 small diameter cryoprobes are routinely used, where the most appropriate active length can be selected according to the actual dimensions of the particular organ. One negative aspect of using this large number of cryoprobes is the increased complexity of surgical planning: consider the difficulty of visualizing the 3D shape of the organ (i.e., the target region), while seeking an optimal layout for as many as 14 cryoprobes, in order to best match the transient temperature field with the imaged freezing front and criteria for cryosurgery success.

It is the opinion of this author that the optimal cryoprobe layout must be obtained with the aid of computerized planning tools, such as those overviewed in Sections 2 through 4 of this manuscript. While the development of a software package for computerized planning relies upon many building blocks, they can all be associated with four key aspects of planning [20]: criteria for optimal cryoprobe layout, duration of the cryoprocure (or, identifying when it is the appropriate time to terminate freezing), automation of planning, and computer runtime.

Criteria for optimal cryoprobe layout: An inherent disagreement exists between the commonly accepted threshold for cryodestruction (the so-called “lethal temperature”) and the monitored parameter during the procedure, which is the freezing front location by means of an imaging technique. In fact, cryoinjury is known to progress within the temperature range bounded by the onset of freezing (at the freezing front) and the lethal temperature. The defect region discussed in Section 4 of this manuscript is one possible concept to quantification of this disagreement. While the existence of a defect region is inherent to the cryoprocure, computerized planning tools may help to minimize its magnitude and control its distribution. The defect region can be further designed to establish safety margins—either externally or internally to the target region. While the overall defect is important in itself, it is not the only important parameter, where many rules can be added to planning, such as the minimum distance between cryoprobes and anatomical features. Setting the most appropriate set of rules for the search after the optimal cryoprobe layout is probably the most significant challenge in cryosurgery planning, once the computation capabilities reviewed in the current manuscript have been demonstrated.

Duration of the cryoprocure: The existence of a defect region for a specific number of cryoprobes plays a critical role in predicting the duration of the procedure. For example, for an organ volume of—say—75 ml (bigger than the size of a typical candidate for such a procedure), the duration of the operation is expected to be between 4 and 18.5 minutes, using as many as 14, to as few as 6 cryoprobes, respectively [18], when all the cryoprobes are operated simultaneously in an optimal layout. While the ratio of the volume below the planning isotherm to the volume of the frozen region is quite low at steady state, actual cryoprocures are ordinarily terminated at the very early stage of the heat transfer process. In fact, several studies suggest that the number of cryoprobes should be increased in order to decrease the internal defect region, which can be concluded from the volume histograms in [23-26]; the termination of cryosurgery occurs earlier with the increasing number of cryoprobes. Selecting the appropriate number of cryoprobes is another significant challenge, which impacts the overall defect, the duration of the procedure, and the cost of the operation.

Automation: Given the possible irregular shape of the target region [28], and the non-steady temperature field developing in this region, the overwhelming amount of data to be considered requires the implementation of automated tools for planning. Towards this goal, the force-field algorithm and the bubble-packing method have been developed, as

reviewed in Section 4, above. While automation is presented as a simplified procedure for the purpose of proof-of-concept, actual cryoprotocols may involve a higher level of complexity, which deserves further developments of computation techniques. The study [26] takes automation one step further by planning the so-called “pullback procedure”, where a two-cycle freezing protocol is executed, and cryoprobes are incrementally retracted between cycles (Fig. 5). More recently, the effect of variable insertion depth of cryoprobes, and variation in cryoprobes length have also been investigated [20].

**Computer runtime:** In order to make computerized planning clinically relevant, it must be carried out within minutes—while the patient is on the operating table—otherwise, the target region may change orientation, deform, or even change size. While the numerical technique presented above (Section 3) can execute the 3D case for a dozen or more cryoprobes in a time scale of one minute, accelerating simulation runtime is always advantageous, where a portion of the computer resources can be used for more in-depth analysis and visualization. While robust commercial codes are available for similar tasks of heat transfer simulation, their runtime is disproportionately longer than the techniques presented above. Accelerating numerical techniques for bioheat transfer simulations will always be beneficial for cryosurgery planning.

The ongoing project reviewed in the current manuscript addresses the above key aspects of planning. In particular, it is demonstrated how the necessary building blocks of a computerized surgical tool are integrated for the application of prostate cryosurgery. These building blocks include a technique for geometric modeling of the target region based on ultrasound imaging, a numerical technique for cryosurgery simulations, and cryoprobe layout planning algorithms (the so-called force-field analogy and the bubble-packing method). Experimental verification of developed computerized means is presented as an integral part of the development process. Figure 5 displays key steps of the process while illustrating some of the information made available to the cryosurgeon.

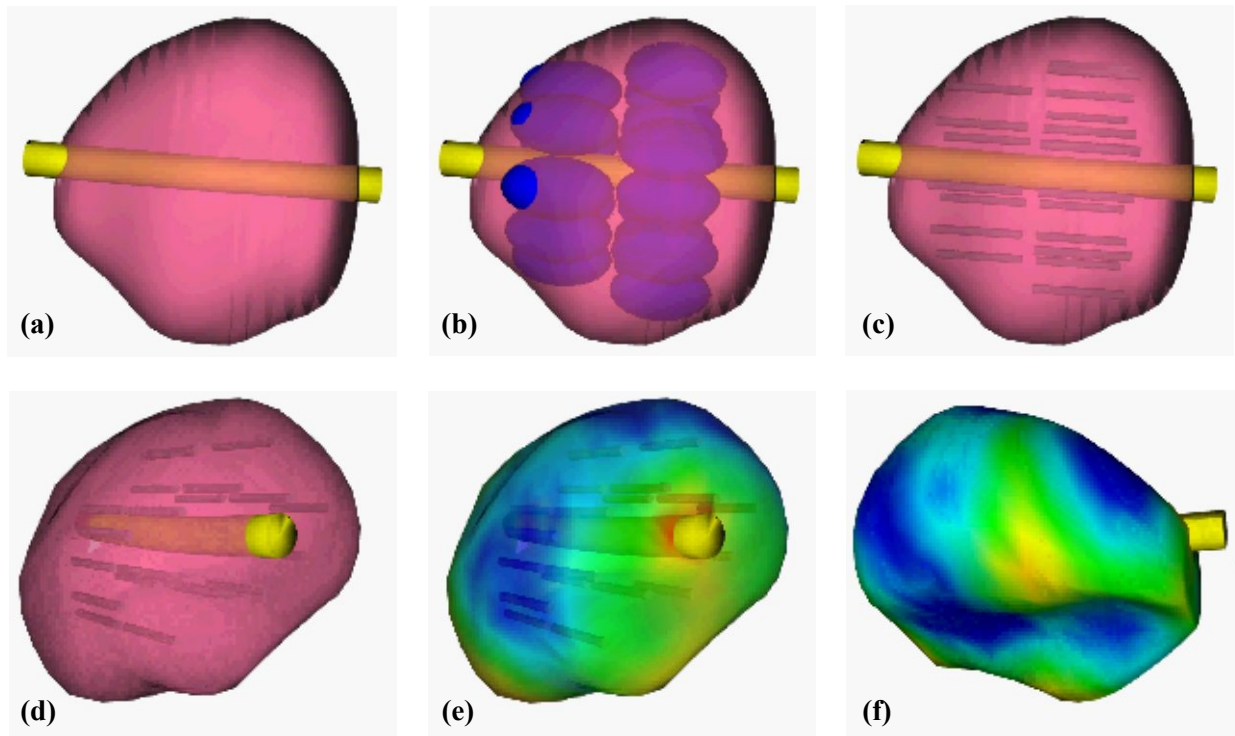


**Figure 5:** Illustration of key steps in computerized planning of a pullback procedure: (a) top view of a reconstructed prostate, (b) top view of bubble-packing results, (c) top-view of cryoprobes placed at the center of bubbles (only active surfaces are shown), (d) tilted view of the same cryoprobe layout, (e) temperature field superimposed on a transparent prostate surface, and (f) temperature field superimposed on a solid prostate surface at a different angle. The yellow conduit is the urethral warmer. Fourteen cryoprobes are simulated in the first freezing cycle, and seven cryoprobes are simulated in the second cycle. Dark blue represents temperatures below the lethal temperature threshold of  $-45^{\circ}\text{C}$  where red represent  $37^{\circ}\text{C}$ . Movies of the process for are posted at [30].

## ACKNOWLEDGEMENT

This work is supported by the National Institute of Biomedical Imaging and Bioengineering (NIBIB) – NIH, Grant No. 1R01EB003563. The author would like to thank Dr. Aaron Fenster of the Robarts Imaging Institute, London, Canada, for providing ultrasound images for this ongoing project.

## REFERENCES

- [1] Baissalov, R., Sandison, G.A., Donnelly, B.J., Saliken, J.C., McKinnon, J.G., Muldrew, K., and Rewcastle, J.C., "A semi-empirical treatment planning model for optimization of multiprobe cryosurgery," *Phys. Med. Biol.* 45, 1085-1098 (2000).
- [2] Baissalov, R., Sandison, G.A., Reynolds, D., and Muldrew, K. "Simultaneous optimization of cryoprobe placement and thermal protocol for cryosurgery," *Phys. Med. Biol.* 46, 1799-1814 (2001)
- [3] Charny, K.C. "Mathematical models of bioheat transfer," in: *Advances in Heat Transfer*, eds. J.P. Hartnett, T.F. Irvine, and Y.I. Cho, Academic Press, 19-156 (1992)
- [4] Cooper, I.S., and Lee, A., "Cryostatic congelation: a system for producing a limited controlled region of cooling or freezing of biological tissues," *J. Nerve Mental Dis.* 133, 259-263 (1961)
- [5] Diller, K.R., "Modeling of bioheat transfer processes at high and low temperatures," in: *Advances in Heat Transfer*, eds. J.P. Hartnett, T.F. Irvine, and Y.I. Cho, Academic Press, 157-358 (1992)
- [6] Gage, A.A., "Cryosurgery in the treatment of cancer," *Surg. Gynecol. Obstet.* 174, 73-92 (1992)
- [7] Keanini, R.G., and Rubinsky, B., "Optimization of multiprobe cryosurgery," *ASME J. Heat Trans.* 114, 796-802 (1992)
- [8] Lung, D.C., Stahovich, T.F., and Rabin, Y., "Computerized planning for multiprobe cryosurgery using a force-field analogy," *Comp. Methods Biomech. and Biomed. Eng.* 7(2), 101-110 (2004)
- [9] Onik, G.M., Cohen, J.K., Reyes, G.D., Rubinsky, B., Chang, Z.H., and Baust, J., "Transrectal ultrasound-guided percutaneous radical cryosurgical ablation of the prostate," *Cancer* 72(4), 1291-1299 (1993)
- [10] Onik, G.M., Gilbert, J.C., Hoddick, W., Filly, R., Callen, P., Rubinsky, B., and Farrel, L. "Sonographic monitoring of hepatic cryosurgery in an experimental animal model," *Am. J. Roentgenol.* 144(5), 1043-1047 (1985)
- [11] Rabin, Y., and Korin, E. "An efficient numerical solution for the multidimensional solidification (or melting) problem using a microcomputer," *Int. J. Heat Mass Tran.* 36(3), 673-683 (1993)
- [12] Rabin, Y., Julian, T.B., and Wolmark, N., "A compact cryosurgical apparatus for minimal-invasive cryosurgery," *Biomed. Instr. & Tech.*, 31, 251-258 (1997)
- [13] Rabin, Y., and Shitzer, A., "Numerical solution of the multidimensional freezing problem during cryosurgery," *ASME J. Biomech. Eng.* 120(1), 32-37 (1998)
- [14] Rabin, Y., and Stahovich, T.F., "Cryoheater as a means of cryosurgery control," *Phys. Med. Biol.* 48, 619-32 (2003)
- [15] Rabin, Y., Lung, D.C., and Stahovich, T.F., "Computerized planning of cryosurgery using cryoprobes and cryoheaters," *Technol. Cancer Res. Treat.* 3(3), 227-243 (2004)
- [16] Reif, F., "Chapter 5– Simple applications of macroscopic thermodynamics," in: *Fundamentals of Statistical and Thermal Physics*. McGraw-Hill. ISBN 07-051800-9 (1965)
- [17] Rossi, M.R., and Rabin, Y., "Experimental verification of numerical simulations of cryosurgery with application to computerized planning," *Phys. Med. Biol.* 52, 4553-4567 (2007)

- [18] Rossi, M.R., Tanaka, D., Shimada, K., and Rabin, Y., "An efficient numerical technique for bioheat simulations and its application to computerized cryosurgery planning," *Comput. Meth. Prog. Bio.* 85(1), 41-50 (2007)
- [19] Rossi, M.R., Tanaka, D., Shimada, K., and Rabin, Y., "Computerized planning of cryosurgery using bubble packing: An experimental validation on a phantom material," *ASME J. Heat Trans.*, 51, 5671-5678 (2008)
- [20] Rossi, M.R., Tanaka, D., Shimada, K., and Rabin, Y., "Computerized planning of prostate cryosurgery using variable cryoprobe insertion depth," *Cryobiology*, in press (2008)
- [21] Rubinsky, B., Gilbert, J.C., Onik, G.M., and Roos, M.S., Wong, S.T.S, Brennan, K.M., "Monitoring cryosurgery in the brain and the prostate with proton NMR," *Cryobiology* 30, 191-199 (1993)
- [22] Schulz, T., Puccini, S., Schneider, J.P., and Kahn, T., "Interventional and intraoperative MR: review and update of techniques and clinical experience," *Eur. Radiol.* 14(12), 2212-2227 (2004)
- [23] Tanaka, D., Shimada, K., and Rabin, Y., "Two-phase computerized planning of cryosurgery using bubble-packing and force-field analogy," *ASME J. Biomech. Eng.* 128(1), 49-58 (2006)
- [24] Tanaka, D., Rossi, M.R., Shimada, K., and Rabin, Y., "Towards intra-operative computerized planning of prostate cryosurgery," *Int. J. Med. Robot. Comp.* 3, 10-19 (2007)
- [25] Tanaka, D., Rossi, M.R., Shimada, K., and Rabin, Y., "Cryosurgery planning using bubble packing in 3D," *Comp. Meth. Biomech. Biomed. Eng.* 11(2), 113-121 (2008)
- [26] Tanaka, D., Rossi, M.R., Shimada, K., and Rabin, Y., "Computerized planning of prostate cryosurgery with pullback operation," *Comput. Aided Surg.* 13(1), 1-13 (2008)
- [27] White, A.C., "Possibilities of liquid air to the physician," *J. Am. Med. Assoc.* 36, 426-9 (1901)
- [28] <http://www.me.cmu.edu/faculty1/rabin/ProstateModelReconstructionF.htm>
- [29] <http://www.me.cmu.edu/faculty1/rabin/ExperimentalVerification.htm>
- [30] <http://www.me.cmu.edu/faculty1/rabin/PullbackModelDF.htm>